Supplementary Figure 1

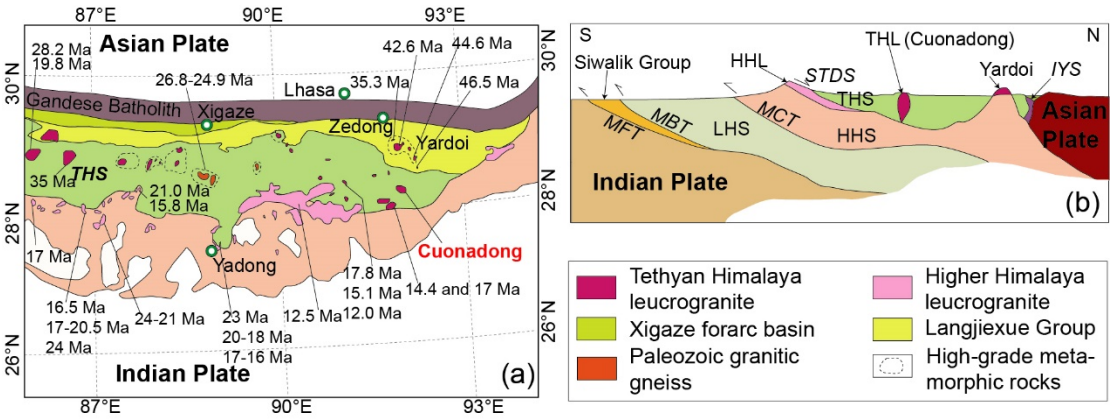

Supplementary Fig. 1 (a) Distribution of the Himalayan leucogranites in the Eastern part of the Himalayan Orogen. Representative age data for the leucogranites were displayed. The age data come from (Cottle et al., 2015; Edwards and Harrison, 1997; Gao et al., 2013; Huang et al., 2017; Liu et al., 2016, 2017; Searle et al., 1997; Shi et al., 2017; Streule et al., 2010; Wu et al., 2020; X.C. Liu et al., 2016; Yu et al., 2011); (b) Cross-section of the Himalayan Orogen showing the location of the Himalayan and Tethyan Himalayan leucogranites (Modified after Wu et al., 2020). STDS: South Tibetan Detachment System; MCT = Main Central Thrust; MBT: Main Boundary Thrust; MFT: Main Frontal Thrust; HHS = High Himalayan Sequence; THS = Tethyan Himalayan Sequence; THL = Tethyan Himalayan leucogranites; HHL = High Himalayan leucogranites.

Supplementary Figure 2

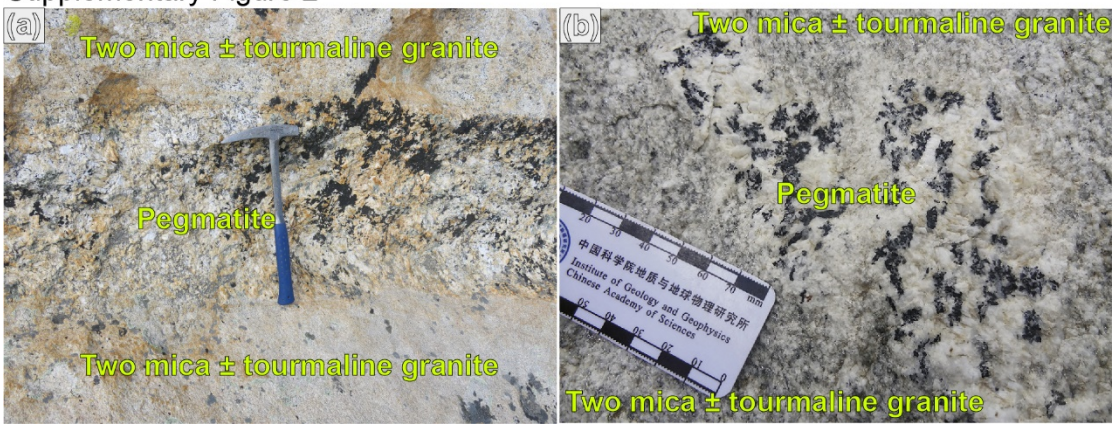

Supplementary Fig. 2 (a) Pegmatite veins in the two mica ± tourmaline granite, without clear boundary between them; (b) Pegmatite pockets in the two mica ± tourmaline granite, without clear boundary between them (after Wu et al., 2020).

Supplementary Figure 3

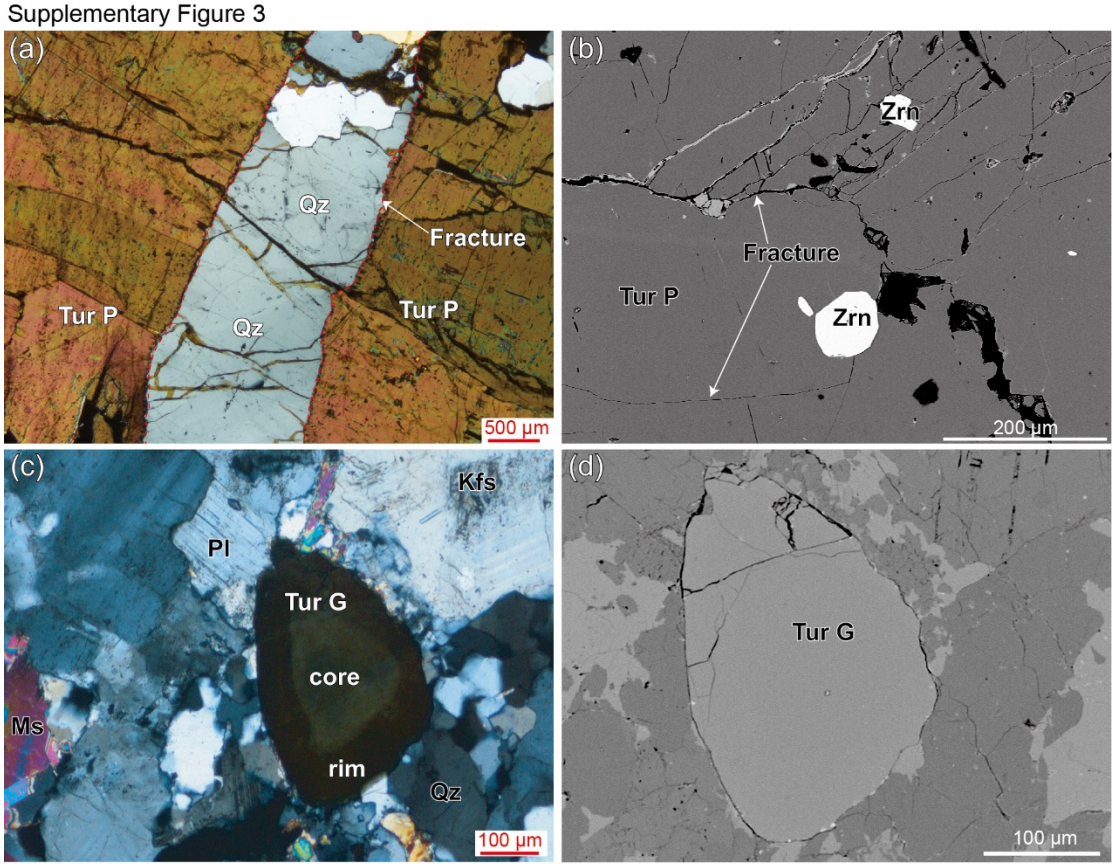

Supplementary Fig. 3 (a) Photomicrograph of the Tur P, which exhibits yellowish-brown colors and is commonly invaded by quartz veins along the fracture; (b) BSE image of the Tur P, showing the existence of fractures in them. Some zircons inclusions could also be observed in the Tur P; (c) Photomicrograph of the Tur G, showing the coexistence of Tur G with muscovite, feldspar and quartz. The Tur G show typical core-rim texture; (d) BSE image of the Tur G. Core-rim texture was not shown under BSE image. Tur = tourmaline, Qz = quartz, Zrn = zircon, Pl = plagioclase, Ms = muscovite, Kfs = k-feldspar.

Supplementary Figure 4

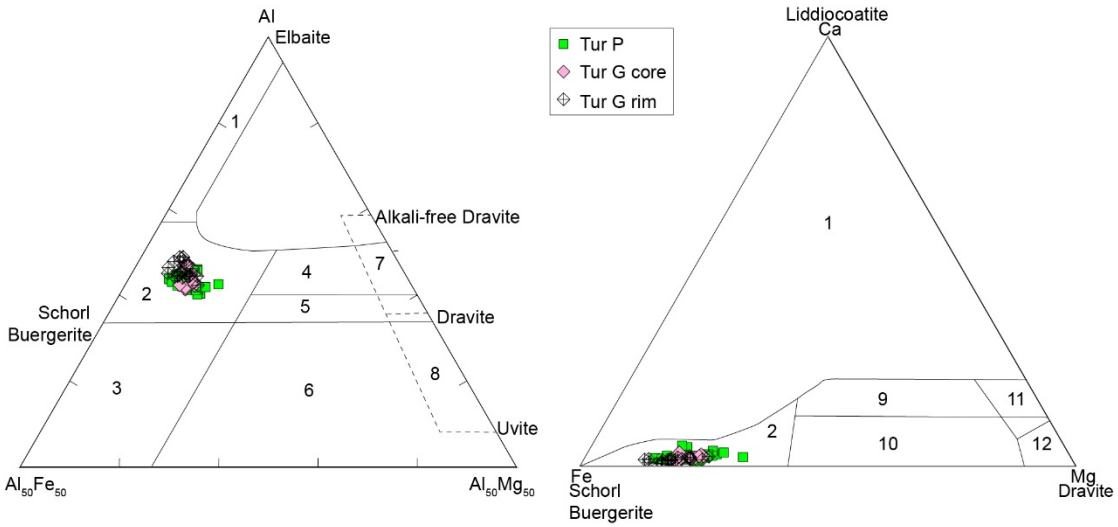

Supplementary Fig. 4 (a) Ternary Al-Fe-Mg and (b) Ca-Fe-Mg diagram showing tourmaline compositions at Cuonadong. The regions define the compositions of tourmaline from different rock types, according to Henry and Gidotti (1985). 1 = Li-rich granitoids and associated pegmatites and aplites; 2 = Li-poor granitoids and associated pegmatites and aplites; 3 = Fe^{3+}-rich quartz–tourmaline rocks (hydrothermall altered granites); 4 = Metapelites and metapsammites coexisting with an Al-saturating phase; 5 = Metapelites and metapsammites not coexisting with an Al-saturating phase; 6 = Fe^{3+}-rich quartz–tourmaline rocks, calc silicate rocks, and metapelites; 7 = Low Ca metaultramafics and Cr, V-rich metasediments; 8 = Metacarbonates and metapyroxenites; 9 = Ca-rich metapelites, metapsammites, and calc-silicate rocks; 10 = Ca-poor metapelites, metapsammites, and quartz–tourmaline rocks; 11 = Metacarbonates; 12 = Metaultramafics.

References:

Cottle, J.M., Searle, M.P., Jessup, M.J., Crowley, J.L., and Law, R.D. (2015) Rongbuk re-visited: Geochronology of leucogranites in the footwall of the South Tibetan Detachment System, Everest Region, Southern Tibet. Lithos, 227, 94–106.

Edwards, M.A., and Harrison, T.M. (1997) When did the roof collapse? Late Miocene N–S extension in the high Himalaya revealed by Th-Pb dating of the Khula Kangri granite. Geology, 25 (6).

Gao, L., Zeng, L.S., Hou, K.J., Guo, C.L., Tang, S.H., Xie, K.J., and Guyue, H.U. (2013) Episodic crustal anatexis and the formation of Paiku composite leucogranitic pluton in the Malashan Gneiss Dome, Southern Tibet. Science Bulletin, 058, 3546–3563.

Henry, D.J., and Guidotti, C.V. (1985) Tourmaline as a petrogenetic indicator mineral: an example from the staurolite-grade metapelites of NW Maine. American Mineralogist, 70, 1–15.

Huang, C.M., Zhao, Z.D., Li, G.M., Zhu, D.C., Liu, D., and Shi, Q.S. (2017) Leucogranites in Lhozag, southern Tibet: Implications for the tectonic evolution of the eastern Himalaya. Lithos, 294-295, 246–262.

Liu, X.C., Wu, F.Y., Yu, L.J., Liu, Z.C., Ji, W.Q., and Wang, J.G. (2016) Emplacement age of leucogranite in the Kampa Dome, southern Tibet. Teconophysics, 667, 163–175.

Liu, Z.C., Wu, F.Y., Ding, L., Liu, X.C., Wang, J.G., and Ji, W.Q. (2016) Highly fractionated Late Eocene (~35Ma) leucogranite in the Xiaru Dome, Tethyan Himalaya, South Tibet. Lithos, 240-243, 337–354.

Liu, Z.C., Wu, F.Y., Qiu, Z.L., Wang, J.G., Liu, X.C., Ji, W.Q., and Liu, C.Z. (2017) Leucogranite geochronological constraints on the termination of the South Tibetan Detachment in eastern Himalaya. Tectonophysics, 721, 106–122.

Searle, M.P., Parrish, R., Hodges, K., Hurford, A., Ayres, M., and Whitehouse, M. (1997) Shisha Pangma Leucogranite, South Tibetan Himalaya: Field Relations, Geochemistry, Age, Origin, and Emplacement. Journal of Geology, 105, 295–318.

Shi, Q.S., Huang, C.M., Lei, H.S., Qi, N.Y., Tong, Y., and Zhao, Z.D. (2017) Geochronology, geochemistry, and petrogenesis of Yamarong leucogranite in Tsona area, Eastern Himalaya, Tibet. Acta Petrologica Sinica, 33, 2454–2466 (in Chinese with English abstract).

Streule, M.J., Searle, M.P., Waters, D.J., and Horstwood, M.S.A. (2010) Metamorphism, melting, and channel flow in the Greater Himalayan Sequence and Makalu leucogranite: Constraints from thermobarometry, metamorphic modeling, and U-Pb geochronology. Tectonics, 29, doi: 10.1029/2009TC002533.

Wu, F.Y., Liu, X.C., Liu, Z.C., Wang, R.C., Xie, L., Wang, J.M., Ji, W.Q., Yang, L., Liu, C., Khanal, G.P., and He, S.X. (2020) Highly fractionated Himalayan leucogranites and associated rare-metal mineralization: Lithos, 352-353, p. 105319, doi: 10.1016/j.lithos.2019.105319.

Yu, J.J., Zeng, L.S., Liu, J., Gao, L.E., and Xie, K.J. (2011) Early Miocene leucogranites in Dinggye area, southern Tibet: Formation mechanism and tectonic implications. Acta Petrologica Sinica, 27, 1961–1972 (in Chinese with English abstract).